Rubbing Effect Analysis in a Continuous Rotor Model

Marcus Varanis[1(✉)], Arthur Mereles[1], Anderson Silva[1],
José Manoel Balthazar[2], and Ângelo Marcelo Tusset[3]

[1] Federal University of Grande Dourados, Dourados, Brazil
marcusvaranis@ufgd.edu.br
[2] Aeronautics Technological Institute, São Paulo, Brazil
[3] Federal Technological University of Paraná, Paraná, Brazil

Abstract. One of the most important malfunction that can cause severe damage in rotating machines is the contact between fixed and rotating parts. The most common sources for rubbing is mass unbalance and instabilities due to fluid-rotor interaction. In this way, this paper presents a continuous rotor model for rubbing applications considering transverse shear, rotatory inertia, and gyroscopic moments. The contribution of it is to present a model to be applied in cases where these effects are not negligible. It is shown that for low slenderness ratio the model is equivalent to the commonly used Euler-Bernoulli continuous model. The normal and friction contact forces between the rotor and the stator are modeled using the Hertz contact theory, which is a nonlinear contact model, and the Coulomb friction model, respectively. In addition, the response of the rotor under impact was studied in the frequency domain using Wavelet Techniques for detection and characterization of rubbing phenomenon.

Keywords: Continuous model · Hertz contact model
Rotor-stator contact · Wavelet transform

1 Introduction

The occurrence of the rubbing phenomenon in a rotating machine is a serious problem that can lead to mechanical failures of the machine components. This phenomenon is seen due to many reasons such as rotor vibrations due unbalance, excessive displacements due to rotor misalignment, rotor permanent bow, or fluid related constant radial forces [1]. In turbomachines, like aircraft engines, rubbing may result from different thermal growth between the rotor and stator and from a blade loss, which induce high displacement due to the huge unbalance created. Investigations on the dynamics of rotating machinery have been made for more than a hundred years. Some primitive models, such as the Jeffcott rotor, consisting of massless shafts with rigid rotors have already been extensively studied [2,3]. Although these primitive rotor models are not suitable for modeling real

rotating machines, they provide an important insight into the physics of rotating systems. The models that are used to predict the properties of real rotating systems consist in flexible or continuous rotor models. In [4], a complete review on rotor models is provided. In order to overcome the difficulties in working with the continuous models, some discretization methods were proposed like transfer matrix method [5] and finite elements methods [6,7]. The early models were made mainly to compute the natural frequencies of the rotating systems, and they were mostly only valid in linear systems. As nonlinear effects have been seen in many experimental procedures [8–10], the models needed to be improved to predict such effects. Some numerical works also presented the occurrence of nonlinear effects in rotating systems [11–18]. These effects were mainly due to oil bearing non-linear characteristics or rubs and impacts in journal bearing systems [19].

An initial study on rubbing was performed by Szcygielski [20], which consisted in a piecewise linear and globally nonlinear model and presented a good qualitative agreement between experimental results. A complete review on rubbing phenomena was performed by Muszynska [21]. Most of the models proposed to describe rotating systems with rub were very simplified lumped mass models, because of the computational problems related to more complex ones due to nonlinear effects. Such models are inadequate because the nonlinear effects excite a wide spectrum band and hence more detailed models need to be considered [19]. Some continuous rotor models are presented in [1,12,13,19,22]. The rubbing forces have a non-smooth behavior in stiffness, which makes the systems exhibit some complicated oscillations. Studies on the rubbing phenomenon showed that the rotating system presented a rich class of nonlinear dynamics such as sub and super-synchronous responses, quasi-periodic responses and chaotic motions [23].

A great number of the rotor models found in the literature are based on the Euler-Bernoulli beam theory. This approach does not take into account the effects of the rotatory inertia and shear deformation of the rotor, which are not significant for slender rotors. However, for rotors with high slenderness ratio, the error in the natural frequencies computed using the Euler-Bernoulli theory are high. The effect of the rotary inertia and shear deformation reduces the fundamental natural frequency by 0.3% in a uniform beam with a slenderness ratio of 1:20, and the effect is bigger for higher modes [24]. Thus, in such cases, the Timoshenko beam theory needs to be applied.

In this work, a continuous rotor model with rubbing is presented. The effects of the rotatory inertia, shear deformation and gyroscopic moments are included in the model. The contact forces are modeled using the Hertz contact theory and the Coulomb friction model. In addition, Wavelet Techniques were applied in the responses to characterize the rubbing in the frequency domain.

2   Background

2.1   Continuous Rotor Model

The model that was studied in this work consists in a continuous rotor model of a thick shaft simply supported at both ends, as depicted in Fig. 1. It is important
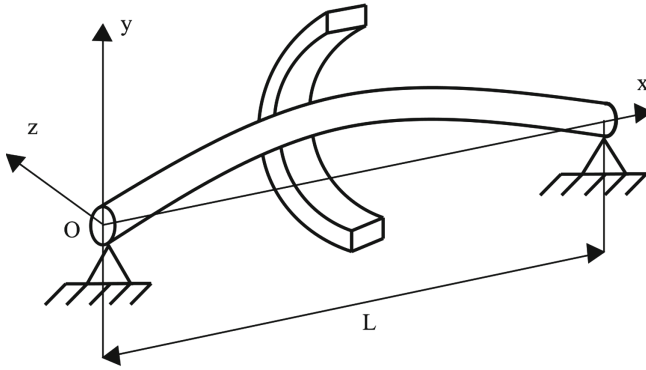
Fig. 1. Schematic representation of the rotor.

to point out that the bearing behavior was not considered in the model, as the boundaries were considered simply supported ends. Although this approach is unrealistic, it was followed to simplify the analysis of the rubbing effect in the vibration model. The equations of motion of the movement of the rotor in the vertical (v) and horizontal (w) directions are written as, respectively [25],

$$
\begin{aligned}
& EI\frac{\partial^4 v}{\partial x^4} - \frac{EI\rho}{\kappa G}\frac{\partial^4 v}{\partial x^2 \partial t^2} + \rho A\frac{\partial^2 v}{\partial t^2} - \rho A r_0^2\left[\left(\frac{\partial^4 v}{\partial x^2 \partial t^2} - \frac{\rho}{\kappa G}\frac{\partial^4 v}{\partial t^4}\right)\right. \\
& \left. + 2\Omega\left(\frac{\partial^3 w}{\partial x^2 \partial t} - \frac{\rho}{\kappa G}\frac{\partial^3 w}{\partial t^3}\right)\right] = F_{u,y}(t)\delta_d(x-a) + F_{c,y}(t)\delta_d(x-a)
\end{aligned}
\tag{1}
$$

$$
\begin{aligned}
& EI\frac{\partial^4 w}{\partial x^4} - \frac{EI\rho}{\kappa G}\frac{\partial^4 w}{\partial x^2 \partial t^2} + \rho A\frac{\partial^2 w}{\partial t^2} - \rho A r_0^2\left[\left(\frac{\partial^4 w}{\partial x^2 \partial t^2} - \frac{\rho}{\kappa G}\frac{\partial^4 w}{\partial t^4}\right)\right. \\
& \left. - 2\Omega\left(\frac{\partial^3 v}{\partial x^2 \partial t} - \frac{\rho}{\kappa G}\frac{\partial^3 v}{\partial t^3}\right)\right] = F_{u,z}(t)\delta_d(x-a) + F_{c,z}(t)\delta_d(x-a).
\end{aligned}
\tag{2}
$$

where x is the axial axis, t is time, E is the Young's modulus, I is the area moment of inertia, ρ is the density, κ is the form factor and has the value $10/9$ for circular cross-sections, G is the shear modulus, A the cross-section area, r_0 is the radius of gyration, Ω is the rotating speed, δ_d is the Dirac delta function and a is the point of application of the forces, which in the model is considered in the middle of the shaft. The forces acting on the rotor are due to unbalance F_u, considered here a point force, and the forces due to the contact F_c. Equations (1) and (2) can be written in a more convenient form by introducing the following dimensionless variables,

$$
v' = \frac{v}{L}, \quad w' = \frac{w}{L}, \quad \tau = \Omega t, \quad \chi = \frac{x}{L}, \quad c^2 = \frac{A\rho L^4 \Omega^2}{EI},
$$
$$
r = \frac{r_0}{L}, \quad \delta = \frac{9}{5}(1+\nu), \quad a' = \frac{a}{L}.
\tag{3}
$$

where L is the length of the shaft and ν is the Poisson's ratio. Applying the relations of Eq. (3) in Eqs. (1) and (2) and rearranging, one may have,

$$
\frac{\partial^4 v'}{\partial \chi^4} - r^2 c^2 (\delta + 1) \frac{\partial^4 v'}{\partial \chi^2 \partial \tau^2} - 2r^2 c^2 \frac{\partial^3 w'}{\partial \chi^2 \partial \tau} + c^2 \frac{\partial^2 v'}{\partial \tau^2} + 2r^4 c^4 \delta \frac{\partial^4 w'}{\partial \tau^3}
$$
$$
+ c^4 r^4 \delta \frac{\partial^4 v'}{\partial \tau^4} = F_{u,y}(\tau) \delta_d(\chi - a') + F_{c,y}(\tau) \delta_d(\chi - a') \tag{4}
$$

$$
\frac{\partial^4 w'}{\partial \chi^4} - r^2 c^2 (\delta + 1) \frac{\partial^4 w'}{\partial \chi^2 \partial \tau^2} + 2r^2 c^2 \frac{\partial^3 v'}{\partial \chi^2 \partial \tau} + c^2 \frac{\partial^2 w'}{\partial \tau^2} - 2r^4 c^4 \delta \frac{\partial^4 v'}{\partial \tau^3}
$$
$$
+ c^4 r^4 \delta \frac{\partial^4 w'}{\partial \tau^4} = F_{u,z}(\tau) \delta_d(\chi - a') + F_{c,z}(\tau) \delta_d(\chi - a'). \tag{5}
$$

The variable c denotes the dimensionless rotational speed, r is the slenderness ratio, and δ denotes the shear influence. The terms in the left side of Eqs. (4) and (5) represent, respectively, the flexural stiffness effect, the transverse shear and rotatory inertia effect, the gyroscopic effect of distributed mass, the lateral inertia effect, the interaction between the transverse shear and gyroscopic effects, and the interaction between the transverse shear and the rotatory inertia effects. The solution of the homogeneous part of Eqs. (4) and (5) are given as follows, respectively,

$$
v'(\chi, \tau) = \sum_{i=1}^{\infty} \phi_i(\chi) \eta_i(\tau) = \sum_{i=1}^{\infty} A_i e^{\alpha_i \chi} e^{j a_i \tau} \tag{6}
$$

$$
w'(\chi, \tau) = \sum_{i=1}^{\infty} \phi_i(\chi) \zeta_i(\tau) = \sum_{i=1}^{\infty} B_i e^{\alpha_i \chi} e^{j a_i \tau} \tag{7}
$$

where $a_i = \omega_i / \Omega$, being ω_i the natural frequency of the i-th mode of vibration of the system, and α_i can be found solving the characteristic equation. The values of α_i, A_i and B_i that satisfy the characteristic equation correspond to a unique value of c. Moreover, the boundary conditions should be used to obtain the system natural frequencies, which will be the values of c that make the determinant of the coefficient matrix of the algebraic system of equations zero and satisfy the characteristic equation [25]. In addition, the natural frequencies of a thick rotor are obtained in [4,26].

2.2   Rotor-Stator Rub Model

In order to model the contact of the rotor with the stator, the Hertz contact theory was used, which states that the relation between the contact force and the indentation are not linear, i.e.,[27]

$$
F = k_h \varepsilon^n \tag{8}
$$

where F is the contact force, k_h is the Hertz stiffness, ε is the indentation, and $n = 3/2$. Despite the good representation of the impact phenomenon given by the relation of Eq. (8), it suffers the limitation of not representing the energy
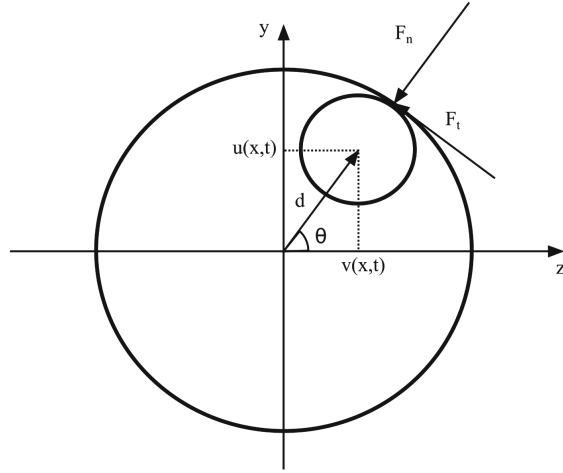
Fig. 2. Contact forces.

dissipated during the impact. To overcome this problem another model was introduced by [28], which has the following form,

$$F = k_h \varepsilon^n + b_h \varepsilon^p \dot{\varepsilon}^q \tag{9}$$

where b_h is the Hertz damping coefficient and the dot represent a time differentiation. It is generally considered that $p = n$ and $q = 1$ [29], thus one can write Eq. (9) as,

$$F = k_h \varepsilon^{3/2}(1 + b_h \dot{\varepsilon}). \tag{10}$$

Figure 2 shows the forces acting on the rotor when impacting the stator. The indentation of the rotor-stator contact will be $\varepsilon = d - g$, being $d = \sqrt{v(x,t)^2 + w(x,t)^2}$ the position of the center of the rotor and g is the gap size. Thus, the magnitude of the normal force for the rotor will be,

$$F_n = k_h(d-g)^{3/2}\left[1 + \frac{b_h}{d}\left(\frac{\partial v(a,t)}{\partial t}v(a,t) + w(a,t)\frac{\partial w(a,t)}{\partial t}\right)\right]. \tag{11}$$

It is worth noting that Eq. (11) is always positive, thus it becomes zero when $d < g$, which means that there is no contact. The horizontal and vertical components of the contact force can be obtained by, respectively,

$$F_{n,y} = -F_n \cos\theta = -F_n\frac{y}{d} \tag{12}$$

$$F_{n,z} = -F_n \sin\theta = -F_n\frac{z}{d} \tag{13}$$

being θ the angle between the rotor's position with relation to the horizontal axis, as shown in Fig. 2. For the tangential force, the Coulomb friction model was used, thus giving,

$$F_t = \mu F_n. \tag{14}$$

where μ is the friction coefficient. Similarly to the normal force, the horizontal and vertical components are obtained by, respectively,

$$F_{t,y} = -F_t \sin\theta = -F_t \frac{z}{d}, \tag{15}$$

$$F_{t,z} = F_t \cos\theta = F_t \frac{y}{d}. \tag{16}$$

2.3 Wavelet Transform

The wavelet techniques have been used to describe the pattern of motion to verified the chaotic systems. The scale parameter is analogous to the concept of scales used in maps, so in small scales we have more compressed Wavelets with rapidly variable details. On large scales, however, there are more enlarged Wavelets, more visible features and slowly changing. In other words, small scales provide good resolution in the time domain, i.e., the temporal information is preserved. While large scales provide good resolution of the frequency domain.

It is possible to find de Continuous Wavelet Transform (CWT) of signal f at time u and scale s. Suppose that $f \in L^2(\mathbb{R})$, then the CWT is defined as,

$$Wf(u,s) := \langle f, \psi_{u,s}^* \rangle \int_{-\infty}^{+\infty} f(t)\psi_{u,s}^* dt \tag{17}$$

where

$$\psi_{u,s}^* := \frac{1}{s}\psi\left(\frac{t-u}{s}\right), \ u \in \mathbb{R}, \ s > 0 \tag{18}$$

The frequency component of the signal f, as regard to the wavelet $\psi_{u,s}$ at time u and scale s, is given by $Wf(u,s)$ [30]. The scalogram of f, denoted by $\wp$, is defined as [30,31]:

$$\wp := \| Wf(u,s) \| = \left(\int_{-\infty}^{+\infty} | Wf(u,s) |^2 \, du\right)^{1/2} \tag{19}$$

Knowing this relationship, it is possible to interpret $\wp(s)$ as the energy of the CWT of f at scale s. The scalogram can be used to detect which is the most representative scales (or frequencies) of the signal f [30]. The term innerscalogram of f at scale s was defined in [30], and is given as:

$$\wp_{inner}(s) := \| Wf(u,s) \|_{J(s)} = \left(\int_{c(s)}^{d(s)} | Wf(u,s) |^2 \, du\right)^{1/2} \tag{20}$$

A great number of applications of the wavelet transform in rotating machines analysis can be found in [31–33].

3   Results and Discussion

In order to solve the differential equations, the Adams-Bashforth-Moulton integration scheme was used. The most commonly used method, the Runge-kutta scheme, was not applicable, since the rotor model takes into account the rotatory inertia, which turns the problem stiff. One of the most important and challenging tasks in simulating continuous systems is the selection of the time step (Δt) and the number of modes (n). The best alternative in selecting Δt is to assuming it as one-tenth of the inverse of the bandwidth of the response [19]. The methodology followed is fixing a time step Δt and obtaining the responses. Then the time-step is then sub-divided as $\Delta t/2$, $\Delta t/4$, $\Delta t/8$, $\Delta t/16$ and the simulations are performed for each time-step. If the responses obtained do not vary much, the time-step is fixed. A similar procedure is performed for the selection of the number of modes, where the number is varied and the responses compared. The time-step and the number of modes selected were $\Delta t = 0.001$ and $n = 3$, respectively.

The parameters necessary for the simulations are listed in Table 1. The geometric parameters of the rotor were chosen so that the effects of a non-slender shaft could be significant. To first study the effect of the impact parameters in the response of the model, the values of the stiffness (k_h), damping (b_h), and the gap distance (g) were varied, obtaining three different cases. The rotating speed was maintained in 1.5 times the first critical speed of the rotor, giving a value of 2.6 kHz. Figure 3 shows the responses of the rotor for the first case, with the parameters as $k_h = 10^3$ N/m$^{3/2}$, $b_h = 10^2$ s/m and $g = 3 \times 10^{-3}$ mm. The black lines in Fig. 3a and 4c correspond to the gap distance. These parameters of stiffness and damping correspond to a soft impact as one can note by the high indentation in the responses. In the second case, the gap distance was increased to $g = 3.5^{-3}$ mm and the other parameters maintained. It is seen that the responses now present a periodic characteristic, as shown in Fig. 4. This characteristic is reached in the permanent regime where the system presents periodic impacts throughout its vibrational motion, as shown in Fig. 4e. By comparing Figs. 3 and 4, one can note as well that, although the frequency of excitation in both cases were the same, the first case presented a higher frequency of

Table 1. Parameters used in the simulations.

Parameter	Variable	Value
Length of the rotor	L	0.4 m
Diameter of the rotor	d	100 mm
Slenderness ratio	r	0.0625
Young's modulus	E	71 GPa
Shear modulus	G	26.2 GPa
Poisson's ratio	ν	0.334
Density	ρ	26.6 N/m^3
Friction coefficient	μ	0.02

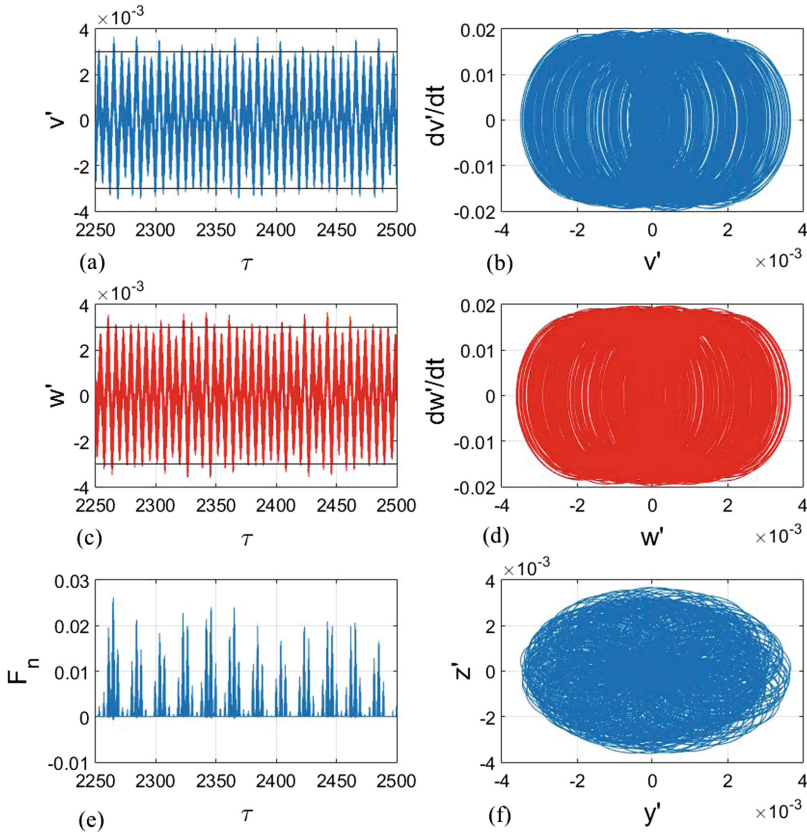**Fig. 3.** Case 1, responses of the model with $k_h = 10^3$ N/m$^{3/2}$, $b_h = 10^2$ s/m and $g = 3 \times 10^{-3}$ mm: (a) horizontal displacement, (b) horizontal state-space portrait, (c) vertical displacement, (d) vertical state-pace portrait, (e) normal contact force and (f) rotor planar trajectory

oscillation. Figure 5 shows the responses obtained for the third and last case, maintaining the other parameters and altering just the Hertz damping coefficient to $b_h = 10^3$. The major difference noted in the responses is the reduction of the contact force, as seen in Fig. 5e. This reduction happens because the coefficient b_h depends inversely on the coefficient of restitution (COR), which is a parameter that represents the energy loss in the impact. Thus as b_h is increased, the impacts tend to be more elastic. Moreover, Fig. 6 presents a comparison between the vertical displacement of the model presented here with no rubbing and a classic Euler-Bernoulli model. As the Euler-Bernoulli model is a model for slender shafts, the slenderness ratio of the model presented here is reduced for a proper comparison. It is seen that the model for the thick shaft represents well a slender one, as one can note by Fig. 6.

Figure 7 presents the application of the Continuous Wavelet Transform (CWT) in the acceleration responses of the model. The CWT was also applied
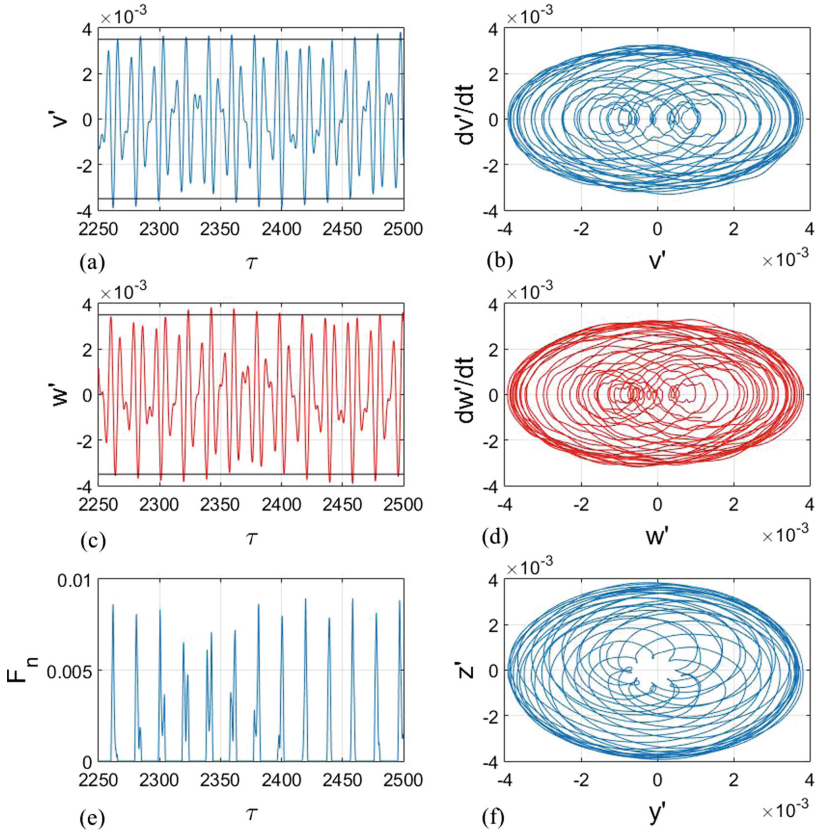
Fig. 4. Case 2, responses of the model with $k_h = 10^3$ N/m$^{3/2}$, $b_h = 10^2$ s/m and $g = 3.5 \times 10^{-3}$ mm: (a) horizontal displacement, (b) horizontal state-space portrait, (c) vertical displacement, (d) vertical state-pace portrait, (e) normal contact force and (f) rotor planar trajectory

in the case with no impact to characterize the rubbing in the responses. The figures show the three natural frequencies of the three modes considered and the frequency of excitation. By comparing the cases with impacts (Figs. 7a, b and c) with the case with no impact (Fig. 7d), it is noted that the rubbing excite a frequency of the rotor at approximately 20 kHz. The most remarkable example of this is presented in Fig. 7a, where no other frequency rather than the 20 kHz appears due to its high energy. This happens because in the Case 1 the rubbing was stronger. A same characteristic is seen in Case 2 (Fig. 7d), where the other frequencies can be seen but a high energy is concentrated in the 20 kHz frequency. In addition, despite the value of the impact force in Case 3 being smaller that the force in Case 2, as discussed before, the spectral energy due to rubbing is higher in Case 3 than in Case 2, the latter which presented little difference comparing with the case with no impact.
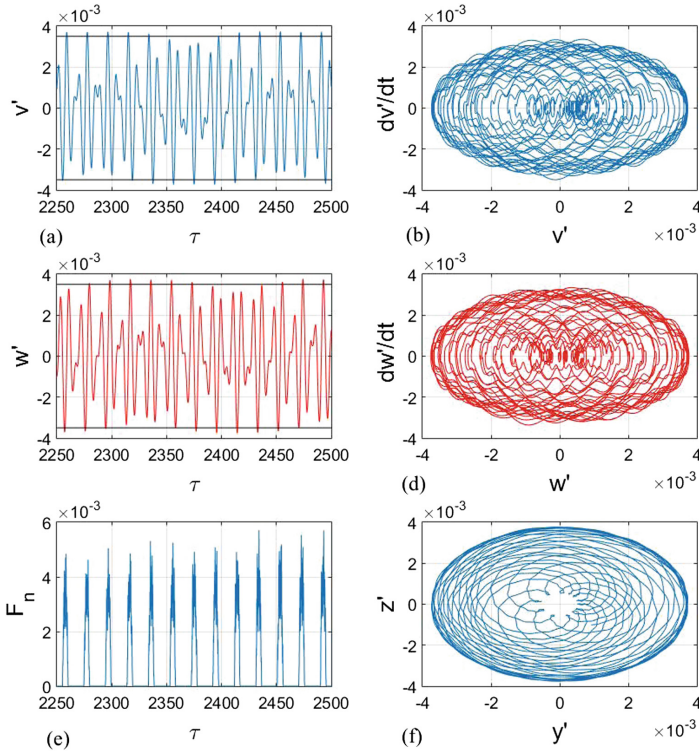
Fig. 5. Case 3, responses of the model with $k_h = 10^3$ N/m$^{3/2}$, $b_h = 10^3$ s/m and $g = 3.5 \times 10^{-3}$ mm: (a) horizontal displacement, (b) horizontal state-space portrait, (c) vertical displacement, (d) vertical state-pace portrait, (e) normal contact force and (f) rotor planar trajectory
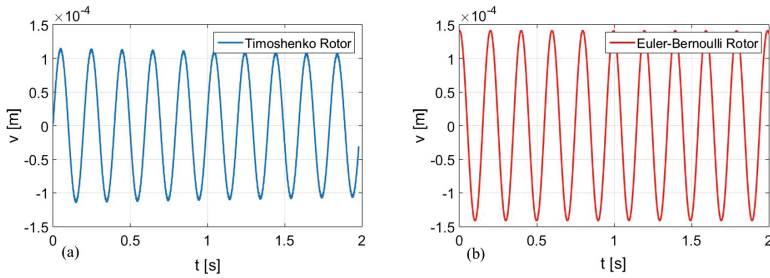

Fig. 6. Comparison between the vertical displacement given by the Timoshenko model proposed and the classic Euler-Bernoulli model for $r = 0.0013$.
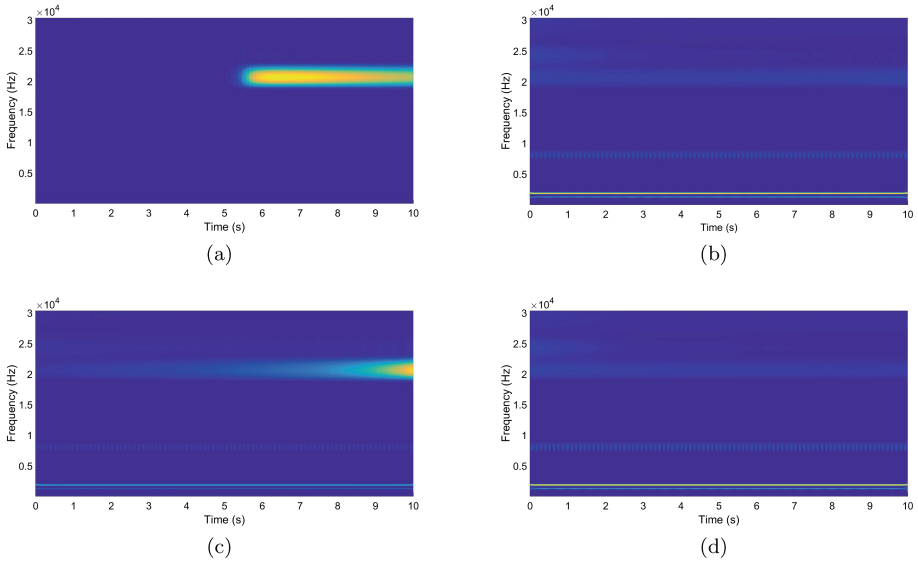
Fig. 7. Application of the CWT in the responses: (a) Case 1, (b) Case 2, (c) Case 3 and (d) Case with no impact.

4   Conclusions

This paper presented a rotor model with rubbing for a shaft with high slenderness ratio. The model considered the effects of the transverse shear, rotatory inertia and the gyroscopic moments. In order to study the rubbing, the impact parameters were studied by varying its values and analyzing the responses given by the system, which presented different characteristics. Also, to validate the model proposed, its responses with no rubbing were compared to the classical Euler-Bernoulli model. In addition, the Wavelet Transform was used to characterize the rubbing in the frequency domain, which is noted by the excitation of a certain rotor frequency.

References

1. Khanlo, H., Ghayour, M., Ziaei-Rad, S.: Chaotic vibration analysis of rotating, flexible, continuous shaft-disk system with a rub-impact between the disk and the stator. Commun. Nonlinear Sci. Numer. Simul. **16**(1), 566–582 (2011)
2. Tondl, A.: Some Problems of Rotor Dynamics. Publishing House of the Czechoslovak Academy of Sciences, Prague (1965)
3. Neilson, R.: Dynamics of electric submersible pumps. In: Rotordynamics 1992, pp. 302–309. Springer, Heidelberg (1992)
4. Eshleman, R., Eubanks, R.: On the critical speeds of a continuous rotor. J. Eng. Ind. **91**(4), 1180–1188 (1969)

5. Raffa, F., Vatta, F.: The dynamic stiffness method for linear rotor-bearing systems. J. Vib. Acoust. **118**(3), 332–339 (1996)
6. Nelson, H.: A finite rotating shaft element using Timoshenko beam theory. J. Mech. Des. **102**(4), 793–803 (1980)
7. Nelson, H., McVaugh, J.: The dynamics of rotor-bearing systems using finite elements. J. Eng. Ind. **98**(2), 593–600 (1976)
8. Ehrich, F.F.: High order subharmonic response of high speed rotors in bearing clearance. J. Vibr. Acoust. Stress Reliab. Des. **110**(1), 9–16 (1988)
9. Ehrich, F.: Observations of subcritical superharmonic and chaotic response in rotordynamics. J. Vib. Acoust. **114**(1), 93–100 (1992)
10. Chu, F., Lu, W.: Experimental observation of nonlinear vibrations in a rub-impact rotor system. J. Sound Vib. **283**(3–5), 621–643 (2005)
11. Muszynska, A., Goldman, P.: Chaotic responses of unbalanced rotor/bearing/stator systems with looseness or rubs. Chaos, Solitons Fractals **5**(9), 1683–1704 (1995)
12. Shaw, J., Shaw, S.: Instabilities and bifurcations in a rotating shaft. J. Sound Vib. **132**(2), 227–244 (1989)
13. Shaw, J., Shaw, S.: Non-linear resonance of an unbalanced rotating shaft with internal damping. J. Sound Vib. **147**(3), 435–451 (1991)
14. Flowers, G.T., Wu, F.: Disk/shaft vibration induced by bearing clearance effects: analysis and experiment. J. Vib. Acoust. **118**(2), 204–208 (1996)
15. Abu-Mahfouz, I.A.: Routes to chaos in rotor dynamics. Ph.D. thesis. Case Western Reserve University (1993)
16. Ishida, Y.: Nonlinear vibrations and chaos in rotordynamics. JSME Int. J. Ser. C Dyn. Control Robot. Des. Manuf. **37**(2), 237–245 (1994)
17. Adiletta, G., Guido, A., Rossi, C.: Chaotic motions of a rigid rotor in short journal bearings. Nonlinear Dyn. **10**(3), 251–269 (1996)
18. Zhao, J., Linnett, I., Mclean, L.: Subharmonic and quasi-periodic motions of an eccentric squeeze film damper-mounted rigid rotor. J. Vib. Acoust. **116**(3), 357–363 (1994)
19. Azeez, M.F.A., Vakakis, A.F.: Numerical and experimental analysis of a continuous overhung rotor undergoing vibro-impacts. Int. J. Non-Linear Mech. **34**(3), 415–435 (1999)
20. Szczygielski, W.M.: Dynamisches Verhalten eines schnell drehenden Rotors bei Anstreifvorgängen. Ph.D. thesis. ETH Zurich (1986)
21. Muszynska, A.: Rotor-to-stationary element rub-related vibration phenomena in rotating machinery. Shock Vib. Dig. **21**, 3–11 (1989)
22. Cveticanin, L.: Resonant vibrations of nonlinear rotors. Mech. Mach. Theory **30**(4), 581–588 (1995)
23. Lahriri, S., Weber, H.I., Santos, I.F., Hartmann, H.: Rotor-stator contact dynamics using a non-ideal drive-theoretical and experimental aspects. J. Sound Vib. **331**(20), 4518–4536 (2012)
24. Inman, D.J.: Engineering Vibration, vol. 3. Prentice Hall, Upper Saddle River (2008)
25. Lee, C.W.: Vibration Analysis of Rotors, vol. 21. Springer, Heidelberg (1993)
26. Jun, O., Kim, J.: Free bending vibration of a multi-step rotor. J. Sound Vib. **224**(4), 625–642 (1999)
27. Půst, L., Peterka, F.: Impact oscillator with Hertz's model of contact. Meccanica **38**(1), 99–116 (2003)
28. Hunt, K., Crossley, F.: Coefficient of restitution interpreted as damping in vibroimpact. J. Appl. Mech. **42**(2), 440–445 (1975)

29. Gilardi, G., Sharf, I.: Literature survey of contact dynamics modelling. Mech. Mach. Theory **37**(10), 1213–1239 (2002)
30. Addison, P.S.: The Illustrated Wavelet Transform Handbook: Introductory Theory and Applications in Science, Engineering, Medicine and Finance. CRC Press, Boca Raton (2017)
31. Yan, R., Gao, R.X., Chen, X.: Wavelets for fault diagnosis of rotary machines: a review with applications. Sig. Process. **96**, 1–15 (2014)
32. Peng, Z., Chu, F.: Application of the wavelet transform in machine condition monitoring and fault diagnostics: a review with bibliography. Mech. Syst. Sig. Process. **18**(2), 199–221 (2004)
33. Chandra, N.H., Sekhar, A.: Fault detection in rotor bearing systems using time frequency techniques. Mech. Syst. Sig. Process. **72**, 105–133 (2016)